

Inspecting Lagrangian coherent structures in turbulent combustion simulations

By V. Nair †, G. Nastac, L. Magri AND M. Ihme

In this study, finite time Lyapunov exponent (FTLE) fields from turbulent reacting flows are evaluated. The unsteady turbulent velocity field is obtained from large-eddy simulations, and reacting (DLR Flame A) and non-reacting unconfined jet configurations are considered. Backward FTLE analysis on the velocity field is performed, and the analysis shows that the ridges approximate the flow structure associated with the organized fluid structure. To examine the merit of this method in identifying coherent structures, we compare the results with the well-known Q-criterion.

1. Introduction

Coherent structures are present even in the most disordered fluid flows (Brown & Roshko 1974). Although visual inspection of the instantaneous velocity fields can identify such structures in certain flow situations, extracting coherent structures from experimental or numerical flow data, especially in the presence of turbulence, has proven to be a challenging task. Coherent structure identification is particularly important in confined reacting flows since such structures often correspond to regions of strong scalar mixing, which controls combustion efficiency and fuel conversion (Ihme *et al.* 2009).

Recently, there has been an increased focus on applying Lagrangian techniques to understand and visualize transport properties in unsteady fluid flows. The advantage of such techniques is that, unlike Eulerian techniques, they are independent of the frame of reference. For instance, in a non-inertial frame of reference, defining vortices as regions filled with closed streamlines can become ambiguous. To provide a frame-independent or objective definition of a vortex, Haller & Yuan (2000); Peacock & Haller (2010) and Haller (2015) recently introduced the framework of Lagrangian coherent structures (LCS) into the field of fluid dynamics. The framework detects coherent structures unambiguously in fluid flows based on how these structures influence flow transport. The methodology identifies material lines that most strongly attract or repel neighboring fluid elements over a selected time interval. A simple heuristic indicator of LCS in fluid flows, known as the finite-time Lyapunov exponent (FTLE) (Haller & Yuan 2000), can be obtained by computing the ridges in the field of the rate of separation of trajectories of neighbouring fluid elements over the time interval. FTLE fields have been used to study a wide range of flows: aerodynamics (Green *et al.* 2011), biological feeding (Peng & Dabiri 2009), ocean and atmospheric transport (Beron-Vera *et al.* 2008) and granular flows (Christov *et al.* 2011), to name a few.

This paper focuses on using the FTLE framework to identify the coherent structures observed in a standard turbulent flame configuration—DLR Flame A. A simulation of the non-reacting case is also performed to compare the structures identified using FTLE.

† Indian Institute of Technology Bombay, India

The coherent structures obtained using FTLE were finally compared with Q-criterion to identify the merits in identifying the shear layer using the novel technique.

2. Formulation and computational setup

The FTLE field is computed by seeding the flow field $\dot{\mathbf{x}} = \mathbf{v}(\mathbf{x}, t)$ with tracer particles and tracking their positions \mathbf{x} in time t . At each location in the flow field, the FTLE is the maximum eigenvalue of the Jacobian of the local flow map $\mathbf{F}_{t_0}^t(\mathbf{x}_0) := \mathbf{x}(t; t_0, \mathbf{x}_0)$, which tracks the displacements of the fluid particles from their starting positions \mathbf{x}_0 over the time interval T . It can then be shown that LCS generally coincides with the ridges of the maximum values in the FTLE field (Haller 2015).

Mathematically, the eigenvalues of the Cauchy-Green strain tensor, which is a 3×3 matrix $\mathbf{C}_{t_0}^{t_0+T}(\mathbf{x}_0, t_0)$, are computed over the time interval as follows

$$\mathbf{C}_{t_0}^{t_0+T}(\mathbf{x}_0, t_0) = \left[\nabla \mathbf{F}_{t_0}^{t_0+T}(\mathbf{x}_0) \right]^* \nabla \mathbf{F}_{t_0}^{t_0+T}(\mathbf{x}_0), \quad (2.1)$$

where ∇ represents the spatial gradient operator with \mathbf{x}_0 and the superscript $*$ refers to matrix transpose. The FTLE field $\sigma_{t_0}^{t_0+T}(\mathbf{x}_0, t_0)$ is then defined as

$$\sigma_{t_0}^{t_0+T}(\mathbf{x}_0, t_0) = \frac{1}{2|T|} \log \left(\lambda_{max} \left[\mathbf{C}_{t_0}^{t_0+T}(\mathbf{x}_0, t_0) \right] \right), \quad (2.2)$$

where the functional λ_{max} corresponds to the largest eigenvalue of the Cauchy-Green tensor $\mathbf{C}_{t_0}^{t_0+T}(\mathbf{x}_0, t_0)$ at each grid location \mathbf{x}_0 from where the individual tracer particles start advecting at time t_0 . It can then be shown that LCS generally coincide with the ridges of the maximum values in the FTLE field $\sigma_{t_0}^{t_0+T}(\mathbf{x}_0, t_0)$ (Haller 2015).

The ridges or the contours of maximum value in the FTLE field for $T > 0$ correspond locally to regions of strongly diverging flow, termed the fFTLE field; in other words, they correspond to material lines responsible for the greatest stretching of fluid parcels. To understand the organizing centers of fluid transport, the computation of FTLE is usually performed backward in time ($T < 0$), hereafter denoted bFTLE. The bFTLE fields when interpreted in forward time are the material lines responsible for particle accumulation or folding of fluid parcels—the local organizing centers in the flow field.

We developed an in-house code to compute the FTLE fields. To validate the results, the FTLE fields for a 2D canonical model of Rayleigh-Bénard convection, that of a time-varying double gyre, were computed. This benchmark case was used to verify the algorithm which will be used to compute the organizing centers in turbulent reacting flow simulations from LES data.

2.1. DLR Flame A

The problem considered is that of a turbulent reacting diffusion flame jet. The jet fuel consists of 22.1% CH_4 , 33.2% H_2 with a nitrogen dilution of 44.7%. The jet ejects to the atmosphere through a pipe of diameter $D = 8.0$ mm at a velocity of $U_{jet} = 42.2$ m/s (corresponding to a Reynolds number of 15200). The stoichiometric mixture fraction for this configuration is $Z_{stoic} = 0.167$. A non-reacting case utilizing this same configuration is also considered for comparison.

The simulations were performed using a low-Mach-number second-order accurate finite difference solver (Pierce & Moin 2001). The setup utilizes a cylindrical structured grid with a computational domain of 120 jet diameters in the axial direction, 45 jet diameters in the radial direction, and 2π radians in the azimuthal direction. The dynamic Germano

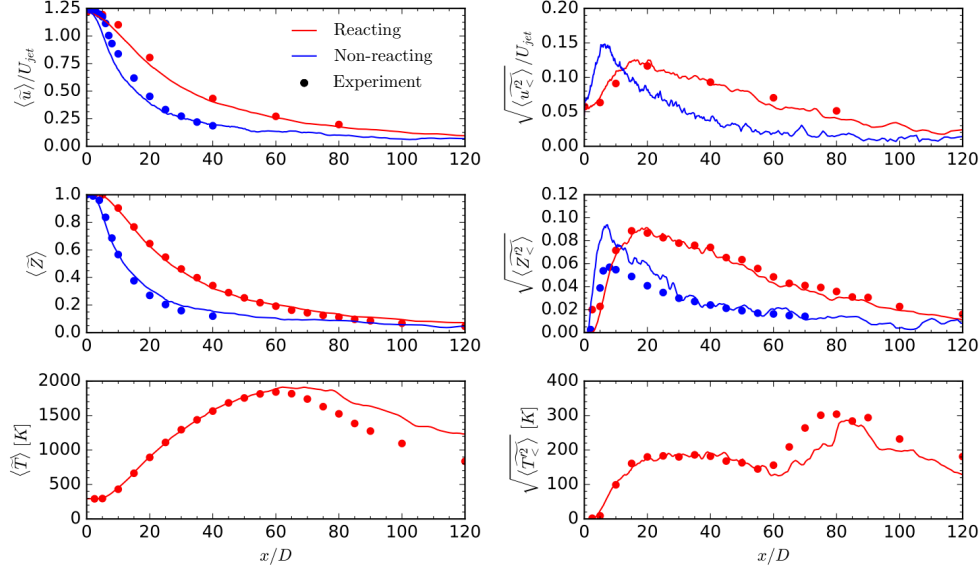


FIGURE 1. Resolved center-line statistics for the two jets for axial velocity, mixture fraction, and temperature compared with experiments by Bergmann *et al.* (1998) and Mi *et al.* (2001).

Diameter	D	0.008 m
Inlet velocity	U	42.15 m/s
Kolmogorov time scale	t_k	33 μ s
Convective time	t_c	$D/U = 189.8 \mu$ s
Time step	dt	0.01 $t_c = 1.9 \mu$ s
Integration time	T	7500 dt (~ 1 flow-through time)
Saving rate	t_s	20 dt = 38 μ s
Data files saved	N	$T/t_s + 1 = 376$
Grid	x,r, θ	$480 \times 181 \times 65 = 5,647,200$

TABLE 1. Important parameters from the simulation. In the code, the coordinates are non-dimensionalized by the jet diameter D and the velocity components by the jet velocity U .

model is employed for the sub-grid scale model. The combustion is modeled and computed using the flamelet progress variable (FPV) approach. Important simulation parameters are summarized in Table 1.

Statistics for the reacting and non-reacting jets are obtained by Favre-averaging azimuthally and in time for approximately five flow-through times. Results are shown in Figure 1. Overall, the statistics agree favorably with the experimental quantities. There is a discrepancy in the temperature after around 60 diameters due to the combustion model and simulation neglecting radiation. Contours and instantaneous snapshots of the flow fields for both cases are shown in Figures 2 and 3. The non-reacting jet demonstrates faster break up and larger fluctuations near the jet exit than the reacting jet. This difference will be further examined and compared using the bFTLE fields.

Since the primary motivation of the project is to test the applicability of the algorithm, the 3D velocity data were reduced to 2D data sets. For the analysis performed in the

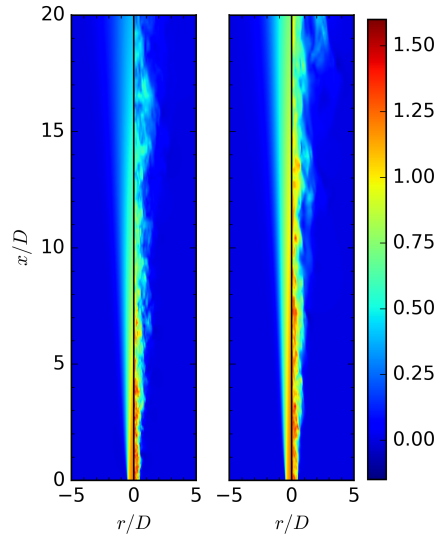


FIGURE 2. Left: Non-reacting jet contour of velocity. Right: Reacting jet contour of velocity. For each case, the left pane displays Favre-averaged values and the right pane displays instantaneous values.

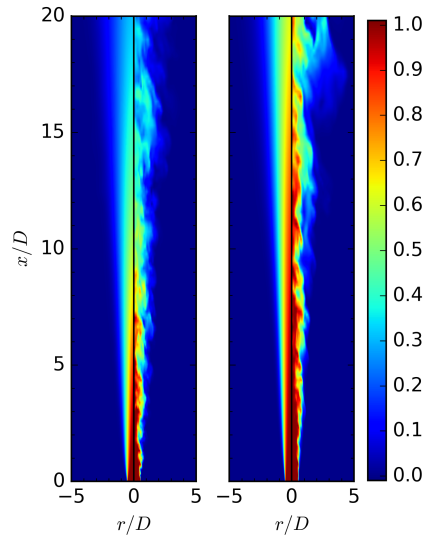


FIGURE 3. Left: Non-reacting jet contour of mixture fraction. Right: Reacting jet contour of mixture fraction. For each case, the left pane displays Favre-averaged values and the right pane displays instantaneous values.

study, 2D slices along an azimuth were generated at each time step through interpolation. This produced a grid of 100×250 in the $r - z$ coordinates. A total of 375 snapshots were obtained corresponding to one flow-through time at a sampling interval Δt of 38

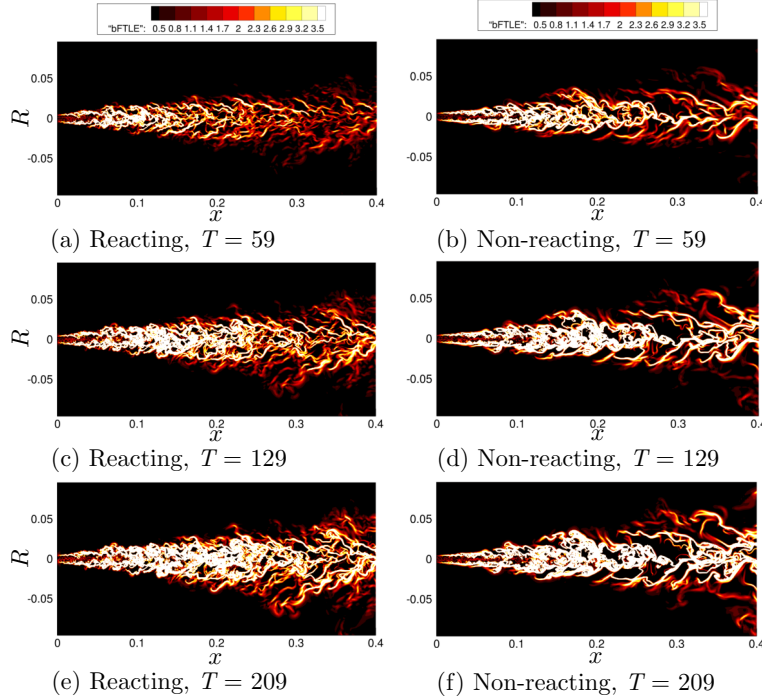


FIGURE 4. Plots of the variation of bFTLE with window lengths T for the reacting and non-reacting simulations.

μs . This simplification was deemed appropriate since the mean properties of the flame are highly axisymmetric. The bFTLE fields were finally computed for these 2D slices.

3. Results

To identify the critical time scales for the reacting and the non-reacting cases, first the bFTLE fields were evaluated for a range of time scales. Figure 4 shows the structures computed at three different time windows T for the reacting and non-reacting cases. The time windows were chosen in a staggered manner to display aperiodic patterns.

In general it is seen that the bFTLE structures become more diffuse as the length of the time window is increased (Figure 4(a,c,e)). This diffusive nature is a result of two effects. First, an increase in the time window results in an accumulation of errors involved in the particle advection algorithm which makes the structures less prominent than the background. Second, as the time interval is increased, the assumption of exponential separation of trajectories which forms the backbone of the bFTLE algorithm becomes invalid. This diffusive nature is more clearly seen for the non-reacting case (Figure 4(b,d,f)). This is as expected since heat release can result in relaminarization effects which tend to make structures more coherent (less diffusive). In other words, the structures are weak compared with the reacting case even at smaller window lengths.

Since identifying relevant time scales are critical to the dynamics of the jet flame, a bFTLE sliding window analysis with window length fixed to T was performed. The choice of the time scale was kept as $T = D/U_{jet}$. The flow field is seeded with tracer particles which start off at the computational node locations in the domain. These particles are

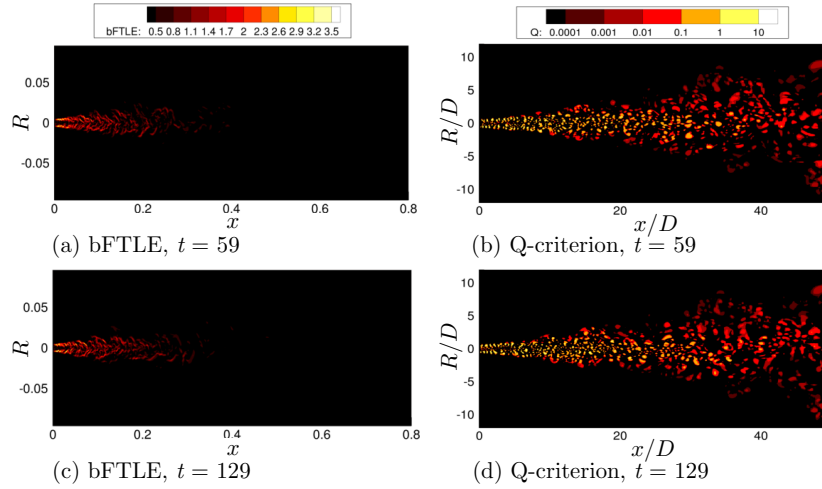


FIGURE 5. Plots of the variation of bFTLE and Q-criterion at two sample instances for the reacting simulation.

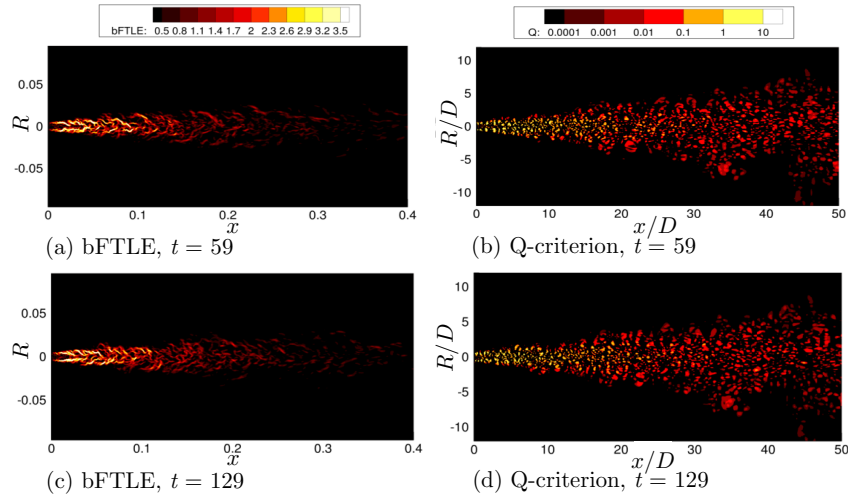


FIGURE 6. Plots of the variation of bFTLE and Q-criterion at two sample instances for the non-reacting simulation.

then advected backward in time using the velocity snapshots at each time instant with an Eulerian back-stepping, using the same sampling time step Δt . The backward integration length T for each mode is chosen to be roughly equal to $1/f$, the frequency of the corresponding dominant peak in the spectra. Once the final particle positions after time T are obtained, the gradients for the Cauchy-Green tensor are computed using a central differencing scheme with a step length of 0.1 mm in either direction from the node. The computation of the bFTLE field is performed until the sum of the time step and the window length T matched the total number of snapshots; i.e., after computing the bFTLE field at time t , the whole procedure is repeated to compute the bFTLE fields at $t + \Delta t$, $t + 2\Delta t$ and so on until the motion of the structures in the bFTLE field over a period of oscillation is captured.

The bFTLE field for the non-reacting case at two sample instances is shown in Figure 5(a,b). The Q-criterion for the flow field computed at the same time instants is also shown (Figure 5(c,d)). It is seen that the shear layer is resolved much better using the bFTLE method than by using the Q-criterion. The Q-criterion, when applied to the flow fields, generates contours which are rather smeared out. On the other hand, the criterion based on bFTLE is able to resolve the shear layer rather satisfactorily. We suspect that the shear layer is captured because the shear layer is the unstable manifold; in other words, it is the layer where the mixing of the fuel and the reactant stream is the strongest. Consequently, the ridges in the bFTLE field coincide with this mixing, in which the reacting layer separates the reactants and the products.

The results for the non-reacting case are shown in Figure 6. The noticeable difference from the reacting case is that the shear layer is more pronounced. However, it is still seen that the bFTLE methodology captures the shear layer rather well. Comparison with the Q-criterion again suggests that it may not be a suitable criterion to identify regions of intense mixing in these scenarios.

4. Conclusions

A novel methodology to identify coherent structures in turbulent reacting flow simulations was performed by extracting the bFTLE fields. The structures were found to be critically sensitive to the FTLE window length. After choosing a window length corresponding to the dominant peak in the centerline point velocity spectra, the structures obtained were compared with the regions of concentrated vorticity identified by the Q-criterion. It was observed that the shear layer was well resolved using the bFTLE framework. A comparison of the structures among the reacting and the non-reacting cases revealed that the structures remain more persistent further downstream for the reacting case.

It is expected that the computation of bFTLE fields will provide a framework to detect flow structures at various frequencies of interest, especially in situations involving transitions to combustion instability, thereby motivating a potential control strategy by designing measures based on the bFTLE field to such detrimental transitions in reacting flow systems.

Acknowledgments

The authors acknowledge use of computational resources from the Certainty cluster awarded by the National Science Foundation to CTR.

REFERENCES

- BERGMANN, V., MEIER, W., WOLFF, D. & STRICKER, W. 1998 Application of spontaneous Raman and Rayleigh scattering and 2D LIF for the characterization of a turbulent CH₄/H₂/N₂ jet diffusion flame. *Appl. Phys. B* **66**, 489–502.
- BERON-VERA, F., OLASCOAGA, M. & GONI, G. 2008 Oceanic mesoscale eddies as revealed by Lagrangian coherent structures. *Geophys. Res. Lett.* **35**, L12603.
- BROWN, G. L. & ROSHKO, A. 1974 On density effects and large structure in turbulent mixing layers. *J. Sound Vib.* **64**, 775–816.
- CHRISTOV, I., OTTINO, J. & LUEPTOW, R. 2011 From streamline jumping to strange eigenmodes: Bridging the Lagrangian and Eulerian pictures of the kinematics of mixing in granular flows. *Phys. Fluids*. **23**, 103302.

- GREEN, M., ROWLEY, C. & SMITS, A. 2011 The unsteady three-dimensional wake produced by a trapezoidal pitching panel. *J. Fluid Mech.* **685**, 117–145.
- HALLER, G. 2015 Lagrangian coherent structures. *Ann. Rev. Fluid Mech.* **47**, 137–162.
- HALLER, G. & YUAN, G. 2000 Lagrangian coherent structures and mixing in two-dimensional turbulence. *Physica D* **147**, 352–370.
- IHME, M., PITSCH, H. & BODONY, D. 2009 Radiation of noise in turbulent non-premixed flames. *Proc. Combust. Inst.* **32**, 1545–1553.
- MI, J., NOBES, D. S. & NATHAN, G. J. 2001 Influence of jet exit conditions on the passive scalar field of an axisymmetric free jet. *J. Fluid Mech.* **432**, 91–125.
- PEACOCK, T. & HALLER, G. 2010 Introduction to focus issue: Lagrangian coherent structures. *Chaos* **20**, 017501.
- PENG, J. & DABIRI, J. 2009 Transport of inertial particles by Lagrangian coherent structures: Application to predator-prey interaction in jellyfish feeding. *J. Fluid Mech.* **623**, 75–84.
- PIERCE, C. D. & MOIN, P. 2001 *Progress-variable approach for large eddy simulation of turbulent combustion*. Tech. Report No. TF-80, Flow Physics and Computational Engineering, Stanford University.